The origin of 4-Vesta's volatile depletion revealed by the zinc isotopic composition of diogenites

Linru Fang, Frederic Moynier, Jean-Alix Barrat, Akira Yamaguchi, Marine Paquet, Marc Chaussidon

GEOCHEMISTRY

The origin of 4-Vesta's volatile depletion revealed by the zinc isotopic composition of diogenites

Linru Fang[1]*, Frederic Moynier[1], Jean-Alix Barrat[2,3], Akira Yamaguchi[4], Marine Paquet[1,5], Marc Chaussidon[1]

Volatile element abundances vary substantially among terrestrial planetary bodies like Earth, Mars, Moon, and differentiated asteroids, leading to intense debate about the governing processes. howardites-eucrites-diogenites (HED) meteorites, most likely from asteroid 4-Vesta, represent highly volatile-depleted Solar System samples, offering critical insights into these processes. Zinc is a moderately volatile element and its isotopic composition reveals sources of volatiles in planetary bodies. Our study finds Zn isotopic anomalies in diogenites overlapping with noncarbonaceous reservoirs, indicating negligible contributions of outer solar system materials to 4-Vesta's volatiles. Besides, zinc isotopic composition of 4-Vesta is lighter than that of chondrites, contrary to the expected signature of evaporation-based volatile depletion. This suggests that after 4-Vesta lost all its volatiles through evaporation during the magma ocean stage, partial kinetic recondensation occurred that produced the observed isotopically light composition. These insights, combined with previous data, underscore the process of global evaporation followed by partial condensation as a key factor influencing the final volatile budget of planetary bodies.

INTRODUCTION

Unraveling the processes governing the origin, distribution and source of volatile elements among solar system materials are fundamental for reconstructing the bulk chemical composition, tracing the thermal history and deciphering the differentiation processes of asteroids and planetary bodies and hold immense potential for elucidating the pathway of the emergence of habitable planets. Highly and moderately volatile elements are defined as elements with a 50% condensation temperature (50% Tc, calculated at a gas pressure of 10^{-4} bar and a reducing oxygen fugacity near that of an early H_2-rich solar gas) below 665 K and between 665 and 1335 K, respectively (*1*). Compared to the bulk solar composition represented by carbonaceous Ivuna-type (CI) chondrites and Ryugu-like materials (*2*, *3*), almost all asteroids and planets in the inner solar system are depleted in volatile elements to various extents (*4*–*6*). Zinc is a moderately volatile element [50% Tc of 730 K (*1*)] and its isotopic composition has been extensively used to elucidate the mechanism of volatile depletion, as well as to uncover the volatile evolution on the Earth, Mars, Moon, and volatile-poor asteroids such as 4-Vesta as represented by howardites-eucrites-diogenites (HED) meteorites (*5*–*8*). However, the variation of the Zn isotopic composition of HED meteorites is quite large [from −7.8 per mil (‰) to +6.3‰ for δ^{66}Zn] and as a result the isotopic composition of 4-Vesta is presently uncertain. One reason is that due to their very low Zn content, HED meteorites are susceptible to terrestrial and/or impactor contamination, especially for brecciated HEDs. The second reason is that the majority of HED meteorites that have been analyzed are eucrites (*5*), basaltic, and cumulate rocks representing the upper crust of 4-Vesta (<12 km below the surface) (*9*), which may have been affected by degassing into vacuum during their formation and therefore may not represent the original composition of 4-Vesta. On the other hand, diogenites are coarse-grained ultramafic rocks dominated by orthopyroxene, thick augite lamellae, and a homogeneous mineral composition, which all indicate a deep-seated origin in the lower crust (*10*, *11*), and their crystallization depth was modeled to be larger than 23 km (*12*). As a result, magmatic degassing is expected to have a limited effect on the Zn isotopic composition of the diogenites (*13*, *14*). However, their Zn content [<1.2 parts per million (ppm), this study] is even lower than that of eucrites [~1.9 ppm, (*15*)], which makes them even more susceptible to contamination, and also even larger samples are required for precise isotopic measurements. Furthermore, previous studies did not perform any leaching procedure that could have removed these potential contaminants (*5*).

In addition to mass-dependent Zn isotope variations, the recent discovery of zinc isotope anomalies of nucleosynthetic origins among solar system materials, with a distinction between outer solar system, CC (carbonaceous), and inner solar system, NC (noncarbonaceous), provides us with a powerful tool to examine the origin of volatile elements in planetary bodies (*16*–*19*). For example, it has been shown that Zn in the Earth has a mixed NC-CC origin (*16*–*18*), while there is no detectable contribution of CC-derived Zn in Mars (*20*, *21*). Thus, Zn isotope anomalies are well suited to trace (i) whether the Zn present in HED meteorites has a common origin and to identify potential terrestrial or impactor contamination and (ii) whether, as observed for refractory elements (*22*, *23*), moderately volatile elements are of NC origin in 4-Vesta.

RESULTS

In this study, we selected 12 diogenites, including falls, hot desert, and cold desert finds. To remove any potential terrestrial contamination, the samples were treated by hot hydrochloric acid leaching. This protocol was proved to be efficient for removing products of terrestrial weathering by notably reducing the Sr, Ba, Zr, and light rare earth element (REE) abundance of weathered diogenites (*24*). Zinc isotopic compositions and concentrations for the paired diogenite leachates and residues are reported in Table 1 and the elemental concentrations of the diogenite residues are displayed in

[1]Université Paris Cité, Institut de Physique du Globe De Paris, CNRS, 1 rue Jussieu, Paris, France. [2]CNRS, IRD, Institut Français de Recherche pour l'Exploitation de la Mer, LEMAR, Univ Brest, Brest, France. [3]Institut Universitaire de France, Paris, France. [4]National Institute of Polar Research, Tokyo, Japan. [5]Centre de Recherches Pétrographiques et Géochimiques de Nancy, CNRS, Université de Lorraine, 15 Rue Notre Dame des Pauvres, 54500 Vandoeuvre-lès-Nancy, France.
*Corresponding author. Email: lfang@ipgp.fr

Table 1. Zinc isotopic compositions and Zn anomalies of diogenites. The suffix "L" in the sample name means the leachate part of the diogenite, and the suffix "R" represents the residue aliquot. Geostandard BHVO-2 was measured in different concentrations (a, 50 ppb; and b, 20 ppb) to monitor the accuracy and the reproducibility of the data under different solution concentrations.

Name	Type	δ^{66}Zn	2SD	δ^{68}Zn	2SD	ε^{66}Zn	2SE	*n*	[Zn] ppm
Tatahouine 1686 PG-L		0.16	0.13					1	
Tatahouine 1635 PE3-L		0.12	0.02	0.31	0.01	−0.35	0.09	4	
Bilanga powder-L		0.01	0.05					1	
Bilanga Px2-L		0.15	0.05					3	
Johnstown-L		−0.40	0.03	−0.81	0.06	0.08	0.09	5	
NWA 5480-L		0.51	0.02					2	
NWA 5484-L		0.00	0.13					4	
Dho 700-L		0.45	0.14					4	
NWA 7831-L		0.33	0.05					2	
SAN 03473,11-L		0.01	0.01	0.01	0.03	0.01	0.04	4	
Y-74097,108-L		0.26	0.13					1	
Y-74013,117-L		0.12	0.05					1	
Y 002875,61-L		0.25	0.05					2	
MIL 090159,5-L		0.15	0.01	0.32	0.01	−0.13	0.01	2	
Tatahouine 1686 PG-R	Fall	1.98	0.08					4	0.10
Tatahouine 1635 PE3-R	Fall	0.47	0.03					5	0.45
Tatahouine 1635 PE3-R replicate	Fall	0.48	0.02	0.97	0.03	−0.09	0.09	1	0.45
Bilanga powder-R	Fall	0.16	0.04					5	0.31
Bilanga Px2-R	Fall	0.23	0.07	0.48	0.14	−0.08	0.16	4	0.34
Johnstown-R	Fall	0.78	0.06	1.56	0.11	−0.11	0.09	4	0.44
NWA 5480-R	Hot desert find	0.84	0.20					4	0.37
NWA 5484-R	Hot desert find	0.08	0.12	0.17	0.20	−0.02	0.23	4	0.40
Dho 700-R	Hot desert find	1.43	0.07	2.88	0.10	−0.30	0.20	4	0.36
NWA 7831-R	Hot desert find	3.14	0.03	6.27	0.04	−0.33	0.14	4	0.18
SAN 03473,11-R	Cold desert find	1.55	0.03	3.07	0.03	−0.08	0.15	4	0.24
Y-74097,108-R	Cold desert find	2.76	0.07	5.52	0.08	−0.37	0.19	4	0.23
Y-74013,117-R	Cold desert find	1.57	0.03					5	0.29
Y 002875,61-R	Cold desert find	2.49	0.01	4.97	0.02	−0.27	0.08	4	0.20
MIL 090159,5-R	Cold desert find	−0.47	0.02	−0.84	0.04	−0.41	0.17	4	1.21
BHVO-2 (a)	Geostandard	0.25	0.04					4	
BHVO-2 (b)	Geostandard	0.25	0.03	0.50	0.03	0.00	0.07	13	

table S1. Repeated analyses of the geostandard BHVO-2 at 50 to 100 parts per billion (ppb) provided an average δ^{66}Zn value of 0.25 ± 0.03‰ (2SD, n = 13). This value is consistent with the recommended δ^{66}Zn value of 0.28 ± 0.09‰ (*25*). The zinc isotope anomaly (ε^{66}Zn) of BHVO-2 is 0.00 ± 0.07‰ (2SE, n =13), which agrees with previous reported value (−0.07 ± 0.15‰) normalized to the same standard (*19*). For measured solutions with lower Zn concentration (<20 ppb), we have exclusively reported the δ^{66}Zn values since diminished signals of ^{68}Zn render the computation of a reliable Zn isotope anomaly unfeasible within the current level of precision. Specifically, for BHVO-2, δ^{66}Zn value is 0.25 ± 0.04‰ (2SD, n =4), which is consistent with the value obtained at 50 ppb.

The average δ^{66}Zn value of the leachates is 0.15 ± 0.12‰ (2SE, n =14), which is consistent with that of Earth's crust component [e.g., $\delta^{66}Zn_{basalt}$ = 0.27 ± 0.04‰, (*26*)]. The δ^{66}Zn values within the diogenite residues display a range from −0.47 and 3.14‰, with cold desert samples encompassing larger spans of Zn isotope variations than hot desert samples (Table 1 and Fig. 1). Among the fall diogenites, two fractions of Billanga exhibit consistent Zn isotopic compositions (δ^{66}Zn = 0.23 ± 0.07‰ and 0.16 ± 0.04‰). In contrast, two fractions of Tatahouine display distinct δ^{66}Zn values of 1.98 ± 0.08‰ and 0.48 ± 0.02‰, which notably differ from a third previously reported data point (δ^{66}Zn = −1.13‰) (*5*).

Despite the broad mass-dependent Zn isotope variations observed in diogenite residues, their mass-independent Zn isotopic compositions remain consistent within errors, but spread from −0.02 ± 0.23‰ to −0.41 ± 0.17‰ (fig. S1A). The calculated average ε^{66}Zn value is −0.21 ± 0.09‰ (2SE, n =10). Spurious isotope anomalies could be a result of nonexponential mass fractionation of the samples (*16*, *27*). To assess this possibility, the Zn isotopic compositions and anomalies corrected using the equilibrium fractionation factor (β = 0.515) were plotted for comparison (fig. S1B). The uncorrelated δ^{66}Zn and ε^{66}Zn corrected by exponential law (R^2 = 0.17, approximate to kinetic fractionation factor; fig. S1A) and the strongly correlated δ^{66}Zn and ε^{66}Zn corrected by the equilibrium fractionation factor (R^2 = 0.79; fig. S1B) suggest that the mass-dependent Zn isotope fractionations of diogenites adhere to the exponential law and are mainly controlled by a kinetic process. It is however possible that the limited variations in ε^{66}Zn values among the diogenites of this study reflect some small unaccounted mass-dependent isotope variations.

DISCUSSION

Effect of contamination

Before assessing the nature of volatile depletion processes on the HED parent body through Zn isotope variations, it is imperative to evaluate potential terrestrial alteration or weathering effects since most diogenites in this study are from either hot or cold (Antarctica) desert regions. Weathered ordinary chondrite finds from hot desert tend to exhibit higher Zn content compared to unweathered samples (*28*). This suggests that alteration processes might have the capacity to reset the Zn isotopic composition of weathered meteorites, especially those with extremely low Zn contents. Notable REE mobilization and Ce anomalies have been observed in Antarctic eucrites and shock-induced cracks appear to be the major conduits for element migration (*29*).

Besides, diogenites exhibit a range of characteristics, encompassing both unbrecciated and brecciated varieties, including monomict and polymict breccias with singular and multiple rock types, respectively. Even within unbrecciated diogenites, signs of shock metamorphism are well documented (*30*, *31*). Thus, exogenous impact contamination can potentially overwrite the elemental and isotopic signatures of diogenites. Elevated highly siderophile element abundances and their flat pattern relative to CI chondrites reflect chondritic impactor contamination during the late accretion stage (*32*). The most prevalent type of chondritic materials found in HED meteorites are CM clasts (*33*). Zinc content in CM chondrites [>130 ppm; (*34*, *35*) and reference therein] is much higher than in HED meteorites [<10 ppm; (*5*)] and even the addition of a small portion of CM clasts has the potential to substantially affect the Zn content and isotopic composition of HED meteorites.

In this context, hot hydrochloric acid leaching is performed to remove possible exotic Zn from the Earth and impactors as both secondary minerals (e.g., carbonates, phosphates, sulfate, sulfides, and weathered silicates) produced by terrestrial weathering and exotic Zn-rich sulfides injected by chondritic impactors can be easily leached out through this process (*24*, *36*). Although samples were treated the same way, the percentages of Zn of individual samples being leached out are quite different (9 to 80%; Table S2 and Fig. 2A), indicating various contaminations they might have experienced. For the leachates of hot desert finds, the Zn/Mg ratios are correlated with S/Mg and K/Mg ratios (Fig. 2, B and C), suggesting that Zn existing in terrestrial weathering products (e.g., sulfates, carbonates, and plagioclases) was leached out. The Fe/Mg and S/Mg ratios for all types of diogenite leachates are well correlated (fig. S2), which suggests that S degassing during sample processing is likely negligible and the measured S contents of diogenite leachates reflect the amounts of sulfides/sulfates. While for cold desert finds, secondary phases might mainly be weathered silicates and phosphates as Zn/Mg and K/Mg and P/Mg ratios (Fig. 2, C and D) of leachates are correlated. The chemical composition characteristics and remarkably consistent δ^{66}Zn values of all the leachates (δ^{66}Zn = −0.40 to 0.51‰) relative to large isotope variation of residues (δ^{66}Zn = −0.47 to 3.14‰) (Table 1) suggest that the leaching process efficiently removed terrestrial alteration.

On the other hand, δ^{66}Zn values of the leachates mostly overlap with the composition of terrestrial rocks (Fig. 1), except for the leachate of Johnstown (Zn proportion is 80% and δ^{66}Zn = −0.40 ± 0.03‰). Meanwhile, contrary to diogenite residues, Johnstown leachate has a positive Zn anomaly (ε^{66}Zn = 0.08 ± 0.09‰; Table 1), indicating that at least some carbonaceous chondritic materials [characterized by positive Zn anomalies; (*16*–*19*)] from the impactors were introduced to the phases dissolved in this leachate. The correlation between Zn/Mg and S/Mg ratios of the leachates for diogenite falls, including Johnstown (Fig. 2B), suggests that the dissolved phases in leachates are mainly sulfides. This observation underscores the efficiency of the leaching process in removing any chondritic impactor contaminations. Consequently, the Zn isotopic composition of diogenite residues will be taken as the most accurate representation of the original composition of the samples.

To assess the potential remaining impactor contamination's influence on the Zn isotopic composition of diogenites residues, we adopt the Zn/Ni ratio as a proxy and CM chondrite as a possible impactor. The calculated average Zn/Ni (0.012) ratio for CM chondrite is derived from the average Zn concentration of 165 ppm [(*37*) and reference therein] and the average Ni content of 13,472 ppm (*38*, *39*). CM chondrites exhibit an average δ^{66}Zn of 0.34 ± 0.02‰

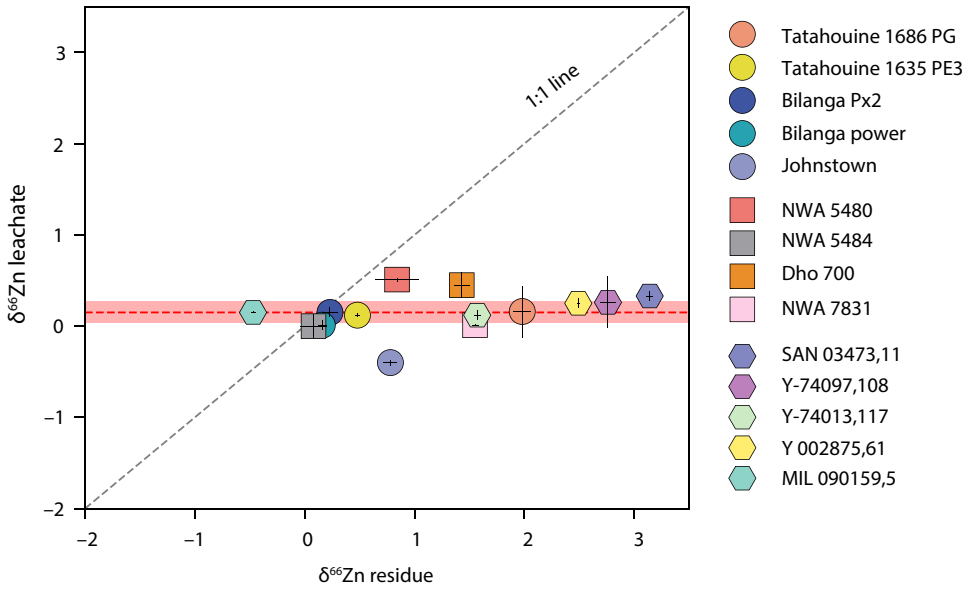

Fig. 1. Paired Zn isotopic compositions of the leachate and residue of a certain diogenite. Circle, square, and hexagon symbols represent diogenite falls, hot desert finds, and cold desert finds, respectively. The red dashed lines show the average Zn isotopic composition of diogenite leachates ($\delta^{66}Zn = 0.15 \pm 0.12‰$) and the shaded field is the corresponding error range. The gray dashed line is a 1:1 line in the plot.

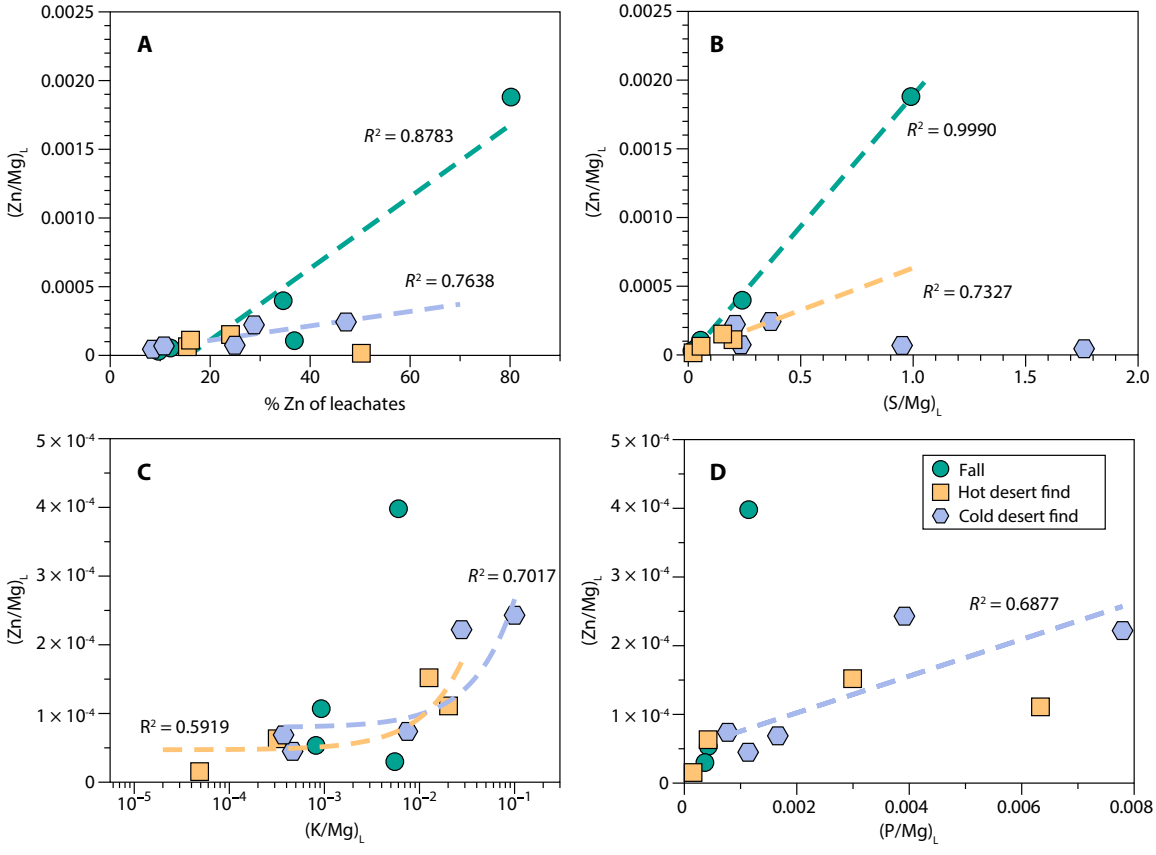

Fig. 2. The geochemistry characteristics of diogenite leachates. (**A**) Zinc percentage and Zn/Mg ratios of diogenite leachates. (**B**) Zn/Mg and S/Mg ratios of diogenite leachates: strong correlations among diogenites falls suggest that Zn exists in sulfides and originated from impactor contamination, while in hot desert finds, Zn-holder could also be weathered sulfates and sulfides. (**C**) Zn/Mg and K/Mg ratios of diogenite leachates suggest that weathered silicates are the main hold for diogenite finds. (**D**) Correlations between Zn/Mg and P/Mg ratios of cold desert finds diogenite leachates indicate their weathered Zn also exists in phosphates.

[2SE, n =18; (*37*)]. In the δ^{66}Zn versus Zn/Ni diagram of diogenite residues, we incorporate the Zn isotopic composition and Zn/Ni ratio of CM chondrite (fig. S3). This plot highlights that the Zn isotopic composition of the diogenites with small Zn/Ni ratios are unlikely to be substantially affected by impactor contamination, as their δ^{66}Zn values far exceed those of CM chondrites (fig. S3). It is noteworthy that there is a negative correlation between Zn isotopic compositions and Zn/Ni ratios of diogenites, and we will discuss below that this reflects evaporation loss of Zn.

Origin of mass-dependent Zn isotope variations among diogenites

Zinc isotopic fractionation during core formation has been found to be negligible (*40*), displaying an estimated range of $\Delta^{66}Zn_{metal\text{-}silicate}$ between −0.05 and 0.12‰ under Vesta's differentiation conditions. In addition, Zn isotopic composition is scarcely affected by magmatic differentiation (<0.1‰ for δ^{66}Zn) (*26*). The crystallization of spinel could at most produce 0.5‰ Zn isotope fractionation during magmatic process (*36*, *41*); however, the Zn content in spinel of HED meteorites are quite low (*42*). Therefore, it appears that core formation and igneous processes cannot explain the considerable variation in δ^{66}Zn (up to 3.5‰) observed among the diogenite residues.

Diogenites are cumulates primarily composed of orthopyroxene along with some olivine, and given their deep-seated origin (*10*, *11*), the potential influence of melt degassing during their crystallization on the Zn isotopic composition is limited. Although, the crystallization of Zn-bearing sulfides such as troilite can contribute to Zn isotope variations in enstatite chondrites (*43*) and iron meteorites (*44*), the portion of troilite in diogenite is minimal and detectable levels of Zn have not been found in troilite of diogenite (*45*). Therefore, the crystallization of sulfide could not account for the Zn isotope variations of the diogenite residues. Our leaching process may inevitably attack some primary troilites and potentially lead to a loss of sulfides, resulting in lighter Zn isotopes enrichments of residues (*46*, *47*). However, the heavier Zn isotopic compositions of the residues compared to the leachates for individual diogenite (Fig. 1) provide us direct evidence substantiating the negligible impact of troilites on Zn isotopic composition of diogenites.

While diogenites were originally thought to have crystallized during the solidification of a magma ocean (*12*, *48*), trace element geochemistry (e.g., Eu anomaly and Dy/Yb ratio) and chemically zoned orthopyroxene of diogenites rather suggest that they are separate plutons, formed by remelting of magma ocean cumulates together with the assimilation of crustal partial melts (*24*, *49*, *50*). The Zn isotopic composition of eucrites varies from δ^{66}Zn = −7.75 to +6.29‰ (*5*). The assimilation of eucritic melts with various Zn isotopic composition could thus change the Zn isotopic composition of diogenites. The investigation of Ca isotope variations of diogenites shows an effect of assimilating less than 10% crustal partial melts (*51*). However, no correlation between Ca and Zn isotopes within diogenites has been observed, and the assimilation process has not been observed for other isotope studies (*52*, *53*). Furthermore, the Zn isotopic composition of diogenite residues is not correlated with incompatible trace element ratios such as Eu/Eu* and (Dy/Yb)n (fig. S4, A and B). The distinct δ^{66}Zn values between two clasts of Tatahouine, an unbrecciated pristine fall meteorite that crystallized from a specific magma pulse, are quite variable (0.48 and 1.98‰, respectively). Despite Tatahouine being unbrecciated, its orthopyroxene mosaicism indicates that it has experienced shock metamorphism (*30*). This observation reinforces the notion that impact-related vaporization events, rather than crustal assimilation, are likely responsible for the large Zn isotopic variations observed among diogenites.

Zinc is a thermally mobile element and over 90% of the Zn of a chondrite can be lost through diffusion and/or desorption in an open system heating event at a temperature of 700°C (*54*–*56*). Furthermore, some naturally heated CM chondrites have lost over 99% of their initial Zn content and are highly isotopically fractionated (*37*). The heating of these metamorphosed CM chondrites occurred recently and impacts in the asteroid are the most likely source of heating (*57*). Mineralogical records on diogenites have shown that excavation events might have occurred in a high temperature environment (1000°C) (*10*, *30*), which is therefore consistent with experimental results and observation in heated chondrites for large Zn loss and isotopic fractionation in the absence of melting. As our leaching protocol effectively removed impact contamination of Ni and Zn, the negative correlation between Zn isotopic composition and Zn/Ni ratios (fig. S3) of diogenites could be the result of a constant Ni content with decreasing Zn content (heavier Zn isotopic composition) during impact heating.

The influence of impact-induced evaporation on Zn abundance and isotopic composition has been well established across planetary materials, encompassing CM chondrites, ureilites, lunar samples, and impact-generated terrestrial rocks (*6*, *37*, *58*–*61*). Building on these observations and using the lightest Zn isotope of diogenite residue determined in this study as the initial reference point, we modeled the evolution of both Zn content and isotopic composition for diogenite throughout an evaporation event following a Rayleigh fractionation function as

$$\delta^{66}Zn = (\delta^{66}Zn_0 + 1000) \times f^{(\alpha-1)} - 1000$$

where $\delta^{66}Zn_0$ is −0.47‰, $[Zn]_0$ = 1.2 ppm, $f = [Zn]/[Zn]_0$, and α represents the isotopic fractionation factor. The theoretical kinetic fractionation factor during the evaporation process was expressed as $\alpha = \sqrt{\frac{m^{64}Zn}{m^{66}Zn}}$,where m^xZn is the mass of the Zn isotope of mass x or of the evaporation phases such as $ZnCl_2$ and ZnS for igneous systems (*62*). Thus, the theoretical isotopic fractionation factor during the evaporation for Zn isotope is between 0.985 and 0.993 within high vacuum. However, empirical determinations spanning tektites, ureilites, and lunar meteorites and experimentally studies show a suppressed α lying between 0.9980 and 0.9998 (*6*, *58*, *60*, *63*–*65*), which was related to the evaporation in a diffusion-limited regime (*58*) or reflecting near-equilibrium conditions (*64*, *65*). The Zn isotopic composition and content of diogenite residues align well with the modeled curves for α values comprised between 0.9980 and 0.9995 (Fig. 3), indicating that the Zn isotopic variations among diogenite correspond to the loss of Zn vapor stemming from thermal metamorphism most likely during impacts on Vesta.

A light Zn isotopic composition for Vesta

The original Zn isotopic composition of diogenites before impact-induced evaporation represents an upper limit of that for bulk silicate Vesta (BSV; $\delta^{66}Zn = -0.47 \pm 0.02$‰), which is enriched in the lighter Zn isotopes compared to the Earth [$\delta^{66}Zn = +0.16 \pm 0.06$‰, (*7*)]. This observation is consistent with the enrichment in the light Zn isotopes of the unbrecciated eucrite with the oldest Ar-Ar ages [PCA 82502; (*5*, *66*, *67*)] (fig. S5). This eucrite was supposed to have been

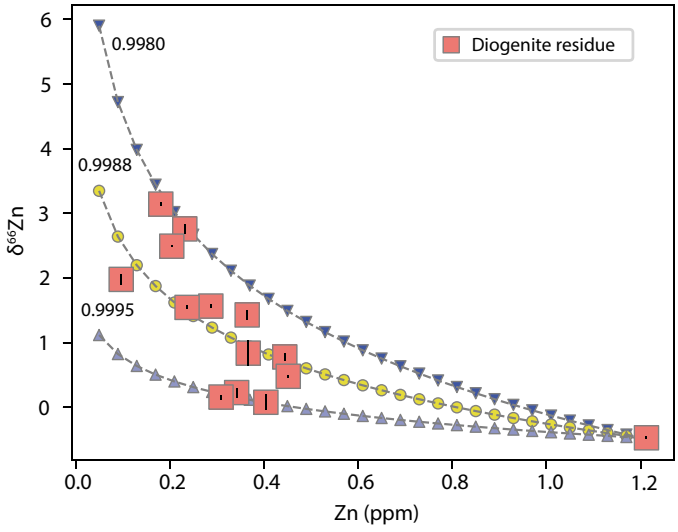

Fig. 3. The evolution curve of the Zn isotopic compositions and contents of diogenites during evaporation loss following a Rayleigh fractionation model. The start point is estimated to be the lightest Zn isotope obtained in this study and the dashed line with inverted triangle, circle, and regular triangle are related to the fractionation factor (α) of 0.9980, 0.9988, and 0.9995, respectively. Zinc isotopic compositions and contents of diogenite residues fit well with α between 0.9980 and 0.9995.

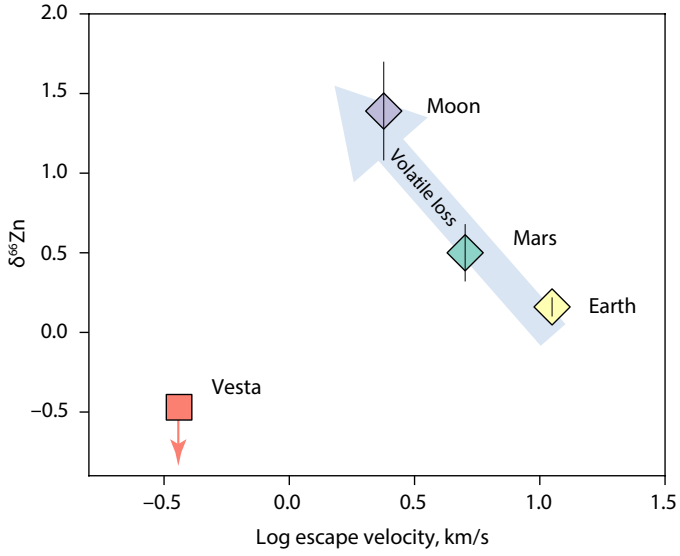

Fig. 4. Zinc isotopic composition and log escape velocity of the Earth, Mars, Moon, and 4-Vesta. Zinc isotope data are from (*6*, *7*, *21*) and this study. The red arrow represents that the Zn isotopic composition of 4-Vesta constrained in this study is an upper limit.

excavated early from the parent body, preserving insights into the original Zn isotopic composition of the Vestan crust.

The Zn content (1.2 ppm) of the most Zn-rich diogenite is over 80 times lower than most chondrites [e.g., $[Zn]_{CI\ chondrite} = 303$ ppm; (*68*)]. Although the low Zn content of diogenite is not unexpected, given the volatile depleted nature of 4-Vesta, the notable enrichment in the lighter Zn isotopes presents a distinctive departure from the conventional trend of volatile depleted planetary materials, which tend to be enriched in the heavier Zn isotopes (Fig. 4). This isotopically light Zn enrichment of 4-Vesta does not align with the correlation observed between the $\delta^{66}Zn$ and the escape velocity for larger bodies such as Earth, Moon, and Mars (Fig. 4). Extreme Zn depletion and light Zn isotope enrichment in 4-Vesta could not be the direct product of nebular accretion since (i) no such precursor has been found to date, even if some chondrules hold light Zn isotope compositions (e.g., Mokoia chondrule, $\delta^{66}Zn = -0.36‰$), their Zn contents are at least 30 times higher than diogenites (*46*); (ii) elevated Mn/Na ratios of HED meteorites compared to chondritic materials indicate that devolatilization happened in an oxidizing rather than reducing environment of the solar nebula since Mn will be relatively less volatile than Na at higher oxygen fugacity (*69*, *70*). Isotopically light and volatile depleted materials were previously observed in angrite meteorites, in the case of K and Rb (*71*, *72*). The light K and Rb isotopic compositions were ascribed to complete evaporative loss followed by kinetic condensation of a small fraction of the original K and Rb budgets (*71*). Zinc is more volatile than K and it was estimated that 4-Vesta lost over 94.2% of its original K budget (*73*), suggesting an even more substantial loss of Zn from 4-Vesta.

Here, we use a simple Rayleigh fractionation to model this kinetic condensation process and the equation can be expressed as

$$\delta^{66}Zn_{BSV} = (1000 + \delta^{66}Zn_0) \times \alpha' \times f^{(\alpha'-1)} - 1000$$

Given the extremely low Zn/Fe ratio of 4-Vesta (less than 7.7×10^{-6}) relative to CI chondrite [1.6×10^{-3}, (*68*)], the extent of recondensation must likely not exceed 1%. Therefore, the fraction (f) of vapor in this context is estimated to lie between 0.99 and 1. Assuming an initial Zn isotopic composition of vapor equivalent to that of CI chondrite [$\delta^{66}Zn_0 = 0.46‰$; (*68*)], the $\delta^{66}Zn_{BSV}$ after condensation is essentially determined by the effective fractionation factor (α′). Taking the upper limit for $\delta^{66}Zn_{BSV}$ to be −0.47‰, we obtained an α′ value of between 0.9990 and 0.9991. This corresponds to an instantaneous Zn isotope fractionation around −1.0‰ between the condensate and vapor phases. Notably, α′ surpasses the ideal kinetic factor (α) of 0.9847 (calculated as $\sqrt{64/66}$). Davis and Richter (*74*) have shown that the isotopic fractionation factor for condensation as a function of partial pressure can be approximated by: $\alpha' - 1 \approx (\alpha - 1) \times (1 - \frac{P_{sat}}{P})$. On the basis of this equation, it would require a vapor saturation of 94% to reproduce the α′ required to explain the $\delta^{66}Zn_{BSV}$. This is consistent with the level (95%) of the saturation estimated during magma ocean setting in asteroid-sized bodies subjected to vapor-melt fractionation (*75*). Consequently, it is conceivable that partial condensation during the magma ocean stage can account for both the light Zn isotope feature and low Zn content for 4-Vesta.

The K and Rb isotope variations are mainly controlled by kinetic processes, and enrichments in the heavy K and Rb isotopes among eucrites were observed (*76*, *77*). The average K isotope composition of eucrites and howardites, which is heavier than the Earth and Mars, was proposed to be representative for the BSV (*76*) and was used to prove that Vesta lost most of its volatiles during evaporation due to its small size and low escape velocity (*78*). However, the large variation of K isotopes among eucrites and howardites could be a result of magmatic degassing and/or impact-induced heating events

after the formation of the Vestan mantle. The large K isotope variations (0.27‰) within individual eucrite fall, Juvinas, suggest in situ impact evaporation (*76*). Similar to Zn isotope composition of eucrites, the average K isotope composition of eucrites and howardites might not represent the BSV, therefore limiting their constraint on the complete history of volatile evolution of Vesta. Besides, K is less volatile than Zn, and the amount of K lost during magma ocean degassing should be smaller than for Zn, so the subsequent partial recondensation inducing the potential light isotope enrichment for K of the Vestan mantle could be hindered. Consistently with the light K and Rb isotopic compositions of bulk silicate angrite (*71*, *72*), the light Zn isotope composition of 4-Vesta further underscores the notion that a sequence of complete evaporation followed by partial recondensation during the magma ocean stage driven by kinetic process represents a pathway that merits substantial attention for its potential to shape the evolution of the moderately volatile elements of asteroids in the inner solar system.

Noncarbonaceous origin of volatile elements in Vesta

The provenance of refractory elements (e.g., REEs, Cr, Ti, Zr, and Ca) within HED meteorites is consistent with that of NC (inner solar system) bodies [e.g., (*22*, *23*, *79*, *80*)]. Similar to these refractory elements, the nucleosynthetic anomaly of moderately volatile element Zn is expected to be homogenized in a magma ocean, and the average ε^{66}Zn value of diogenites ($\varepsilon^{66}Zn = -0.21 \pm 0.09$‰, 2SE) represents the Zn anomaly of the BSV. Notably, this value is intermediate between ordinary chondrites ($\varepsilon^{66}Zn = -0.16 \pm 0.03$‰) and ureilites ($\varepsilon^{66}Zn = -0.26 \pm 0.02$‰) and much more negative than the Earth (Fig. 5). The variations of isotope anomalies of refractory elements among planetary bodies and asteroids were proposed to be the result of mixing of CI chondrite–like materials and ureilite-like materials to different degrees [e.g. (*79*)]. To assess whether it is the case for Zn isotope anomaly, we compared the ε^{66}Zn values with ε^{48}Ca, ε^{54}Cr, and ε^{50}Ti for chondrites and planetary bodies (Fig. 6). Using a simple two-member mixing model, we calculated the evolution curve of ε^{66}Zn values with a starting end-member of an ureilite-like isotope anomalies and an ordinary-like elemental composition mixing with different fractions of CI chondrite–like materials. The equations are shown in Fig. 6 caption, and the parameters of the end-members are listed in table S3. Vesta does not plot on the mixing curve, suggesting that at the difference with refractory elements, mixing between CI-like material and ureilite-like materials cannot account for the observed Zn anomaly for Vesta.

Considering the ε^{66}Zn values alone and assuming that the noncarbonaceous reservoir has an original ε^{66}Zn value similar to the ureilite given that it holds the most negative Zn anomaly among NC meteorites, the possible volatile contributions of CC materials to Vesta is estimated following: $f_{CC}\,(Zn)_{BSV} = (\varepsilon^{66}Zn_{BSV} - \varepsilon^{66}Zn_{NC}) / (\varepsilon^{66}Zn_{CC} - \varepsilon^{66}Zn_{NC}) \times 100$. In this equation, $f_{CC}\,(Zn)_{BSV}$ is the mass fraction of Zn derived from CC reservoir, which calculated to be 8 ± 14%. Assuming that the Zn content of the Vestan mantle is equal to that of the bulk Vesta, as suggested for Mars (*20*), the mass fraction of the CC materials present in Vesta can be estimated by $f_{CC} = [Zn]_{BSV}/[Zn]_{CC} \times f_{CC}\,(Zn)_{BSV}$. Incorporating the mantle Zn concentration for Vesta of 1.2 ppm (it should be noted that this represents the lower limit constrained by this study), the f_{CC} is estimated to be 0.03 ± 0.06% and 0.09 ± 0.20% for a CI and a CV material injection, respectively. This estimate suggests that Zn, and possibly other moderately volatile elements within 4-Vesta, originates purely from the inner solar system reservoirs with minimal contributions from outer solar system materials.

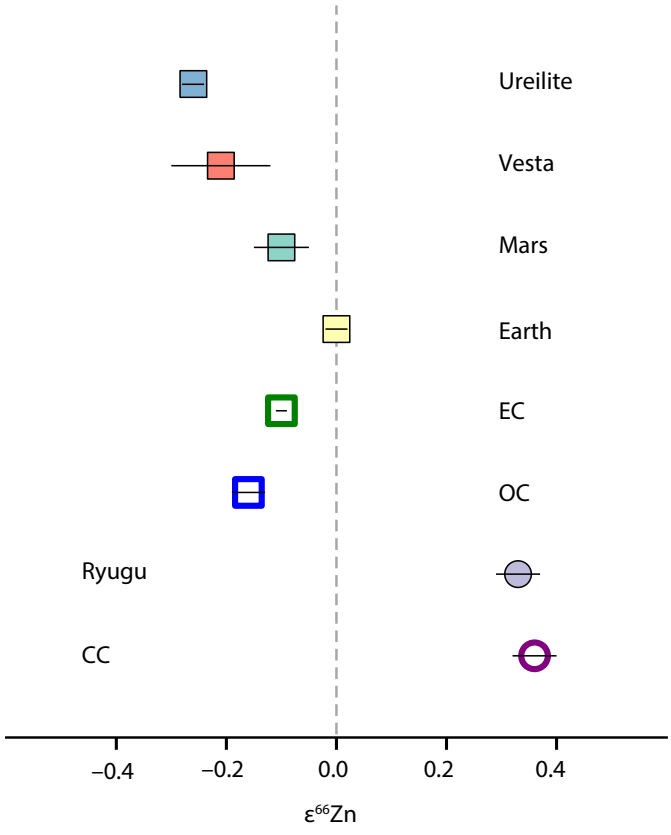

Fig. 5. Zinc isotope anomalies (ε^{66}Zn) of carbonaceous chondrite, ordinary chondrite, enstatite chondrite, Earth, Mars, Ryugu, Ureilite, and 4-Vesta. Data are from (*16*, *17*, *19*–*21*) and this study. All published Zn data relative to standard SRM683 were corrected by a magnitude of 0.07‰ since the ε^{66}Zn values for geostandard BHVO-2 relative to SRM683 and JMC-Lyon are −0.07 ± 0.02‰ (*17*) and 0.00 ± 0.07‰ (this study), respectively. The gray dashed line represents an $\varepsilon^{66}Zn = 0$ for the terrestrial rocks. CC, carbonaceous chondrite; OC, ordinary chondrite; EC, enstatite chondrite.

Planetary bodies, including the Earth, have been proposed to accrete their volatiles by pebble accretion theory where pebbles are composed of millimeter-size chondrules and primitive dust aggregation (*81*). The radial drift of the pebbles from the outer solar system matches the nucleosynthetic anomaly of refractory element Ca well (*79*); however it is debated for other refractory elements (*82*). Regarding the exceedingly negative Zn isotope anomaly and thus the negligible contribution of the volatile from CC reservoirs to 4-Vesta, if the pebble accretion is the mechanism for planetesimal growth, the origin of the 4-Vesta is more likely to predate the potential era of pebble accretion or that alternatively, the pebbles were thermally processed in the planetesimals envelops (*83*).

MATERIALS AND METHODS

Twelve orthopyroxene clasts or powders of diogenite have been carefully selected. This selection includes three falls (Johnstown, Tatahouine, and Bilanga), four hot desert finds (NWA 5480, NWA 5484, Dho 700, and NWA 7831), and five cold desert finds

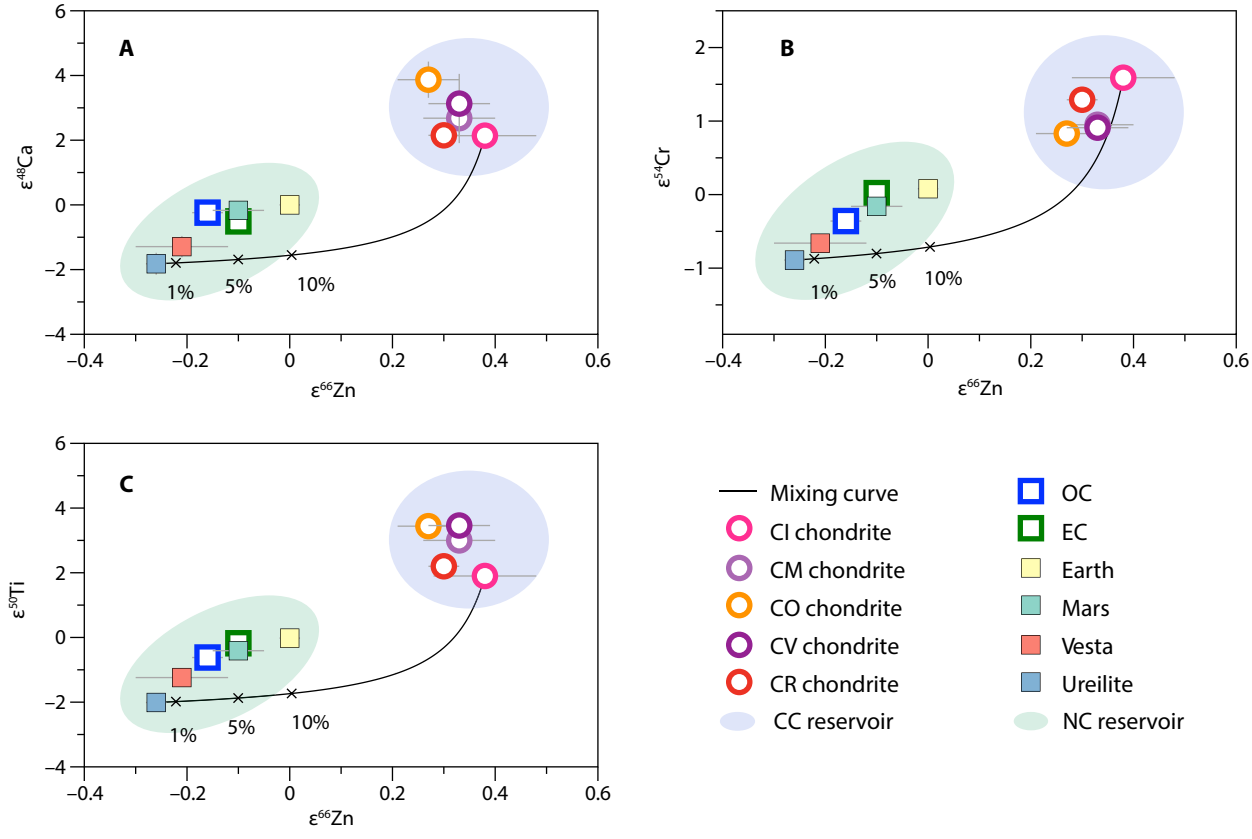

Fig. 6. Relations of Ca, Cr, Ti, and Zn isotopic anomalies among carbonaceous (CI, CM, CO, CV, and CR) chondrites, OC, EC, Earth, Mars, Ureilite, and 4-Vesta. (**A**) to (**C**) show ε^{66}Zn versus ε^{48}Ca, ε^{54}Cr, and ε^{50}Ti of terrestrial samples and meteorites, respectively. The mixing curve of each panel is based on a mass balance calculation, where for a given mass fraction of CI chondrite (f_{CC}), the mixture follows: $[N]_m = f_{CC} \times [N]_{CI} + (1 - f_{CC}) \times [N]_{NC}$; $[\varepsilon^X N]_m = [\varepsilon^X N]_{CI} \times f_{CC} \times ([N]_{CI} / [N]_m) + [\varepsilon^X N]_{NC} \times (1 - f_{CC}) \times ([N]_{NC} / [N]_m)$; where $[N]_m$, $[N]_{CI}$, and $[N]_{NC}$ represent the element concentrations of N (i.e., Zn, Ca, Cr, and Ti) for the mixture, CI end-member and NC end-member, respectively; $[\varepsilon^X N]_m$, $[\varepsilon^X N]_{CI}$, and $[\varepsilon^X N]_{NC}$ represent isotope anomaly of element N for the mixture, CI end-member, and NC end-member, respectively. The parameters of end-members can be found in table S3 and all raw data and their source are compiled in table S4. The error bars are plotted as 2SE (twice SE) and not seen ones are smaller than the sample symbols. Similar plots and calculations have been conducted in previous Zn anomaly work on Earth and Mars (*17*, *20*).

(Y-74097,108; Y-74013,117; Y 002875,61; SAN 03473,11; and MIL 090159,5). Diogenite are cumulates mainly composed of magnesian orthopyroxene with various olivine modal abundance (0 to 30 vol %). NWA 5480 is the sole representative in the olivine-orthopyroxenitic diogenite subgroup, which contains more than 10 vol % olivine (*31*). In addition to magnesian orthopyroxenes and olivine, minor components within these diogenites include plagioclase, high-Ca pyroxene, silica phase, troilite, and metal.

The diogenite clasts (>500 mg) were ground into fine powders using a boron-carbide mortar. To eliminate secondary phases such as rusts and carbonates, a hot 6 N HCl (130°C, 30 min) leaching process was used. The effectiveness of this leaching process was verified by accurately analyzing the REE content of diogenites (*24*, *49*). The resulting residues were rinsed five times with ultrapure water, followed by dissolutions in screw-top Teflon vessels using a concentrated mixture of HF and HNO_3 acid at 130°C on a hotplate for 5 days. Samples were dried down at 110°C and a reheat process with 6 N HCl at 130°C was performed to remove any remaining fluorides. A small aliquot was extracted for measurements of elemental concentrations. The Ca, Ti, and trace element concentrations of diogenite residues were measured at the Institut Universitaire Européen de la Mer, Plouzané using a magnetic sector Thermo Element XR inductively coupled plasma–mass spectrometer following the method in (*15*, *49*). The reproducibility is much better than 5% for trace elements, except Nb. Concentrations of Fe, Mg, and Al for diogenite residues and of Zn, Sr, Ba, S, K, P, Mg, and Fe of diogenite leachates were determined by Agilent 7900 ICP-QMS housed at Institut de Physique du Globe de Paris (IPGP).

The major aliquots of the leachates and residues were dried down at 110°C and converted to 1 or 2 ml of 1.5 N HBr medium, respectively. Chemical purifications for Zn followed the procedure of (*47*, *84*) using home-made Teflon columns filled up with AG-1X8 (200 to 400 mesh) exchange resin. After cleaning the resin with alternating cycle of 0.5 N HNO_3 and MQ water, the solutions of diogenite residues were loaded on long columns (~500-μl resin) and the Zn was collected with 0.5 N HNO_3 after the elution of matrix elements with 1.5 N HBr. The short columns (~100-μl resin) were used two or three times under the similar procedure for the diogenite leachates and Zn cut of diogenite residues to further remove impurities.

Zinc isotope ratios were determined using a Thermo Scientific Neptune Plus multicollector inductively coupled–plasma

mass spectrometer at IPGP. An Apex HF introduction system was used to improve the strength of signals. The diogenite residues and leachates with the highest Zn content were measured in 0.5 N HNO_3 with Zn concentration of 50 to 100 ppb, while the leachates with low Zn content and one of the Tatahouine residue were measured at 10 to 20 ppb. USGS geostandard BHVO-2 was analyzed to monitor the accuracy and the reproducibility of the Zn isotope data. Sample standard bracketing method is used to correct the instrumental fractionation during the measurement. Mass-dependent Zn isotopic composition are reported as the part per 1000 deviation from the JMC-Lyon standard: $\delta^{x}Zn = [(^{x}Zn/^{64}Zn)_{sample} / (^{x}Zn/^{64}Zn)_{JMC\text{-}Lyon} - 1] \times 1000$, where x is 66 or 68 (*25*). Zinc isotope anomalies are expressed as part per 10,000 deviation from the same standard: $\varepsilon^{66}Zn = [(^{66}Zn/^{64}Zn)_{sample} / (^{66}Zn/^{64}Zn)_{JMC\text{-}Lyon} - 1] \times 10000$), with the $^{66}Zn/^{64}Zn$ ratio normalized to a $^{68}Zn/^{64}Zn$ ratio of 0.3856 (*85*) using an exponential law to correct for mass-dependent isotopic fractionation (*16*). The uncertainties of mass-dependent Zn isotopic composition are given as the 2× SD (2SD) and that of mass-independent Zn isotope fractionation are expressed as 2× SE (2SE).

Supplementary Materials

This PDF file includes:

Figs. S1 to S5
Tables S1 to S3
Legend for table S4

Other Supplementary Material for this manuscript includes the following:

Table S4

REFERENCES AND NOTES

1. K. Lodders, Solar system abundances and condensation temperatures of the elements. *Astrophys. J.* **591**, 1220–1247 (2003).
2. J. T. Wasson, G. W. Kallemeyn, Compositions of chondrites. *Philos. Trans. R. Soc. Lond. A* **325**, 535–544 (1988).
3. T. Yokoyama, K. Nagashima, I. Nakai, E. D. Young, Y. Abe, J. Aléon, C. M. Alexander, S. Amari, Y. Amelin, K. I. Bajo, M. Bizzarro, A. Bouvier, R. W. Carlson, M. Chaussidon, B. G. Choi, N. Dauphas, A. M. Davis, T. Di Rocco, W. Fujiya, R. Fukai, I. Gautam, M. K. Haba, Y. Hibiya, H. Hidaka, H. Homma, P. Hoppe, G. R. Huss, K. Ichida, T. Iizuka, T. R. Ireland, A. Ishikawa, M. Ito, S. Itoh, N. Kawasaki, N. T. Kita, K. Kitajima, T. Kleine, S. Komatani, A. N. Krot, M.-C. Liu, Y. Masuda, K. D. McKeegan, M. Morita, K. Motomura, F. Moynier, A. Nguyen, L. Nittler, M. Onose, A. Pack, C. Park, L. Piani, L. Qin, S. S. Russell, N. Sakamoto, M. Schönbächler, L. Tafla, H. Tang, K. Terada, Y. Terada, T. Usui, S. Wada, M. Wadhwa, R. J. Walker, K. Yamashita, Q.-Z. Yin, S. Yoneda, H. Yui, A.-C. Zhang, H. C. Connolly, D. S. Lauretta, T. Nakamura, H. Naraoka, T. Noguchi, R. Okazaki, K. Sakamoto, H. Yabuta, M. Abe, M. Arakawa, A. Fujii, M. Hayakawa, N. Hirata, N. Hirata, R. Honda, C. Honda, S. Hosoda, Y.-I. Iijima, H. Ikeda, M. Ishiguro, Y. Ishihara, T. Iwata, K. Kawahara, S. Kikuchi, K. Kitazato, K. Matsumoto, M. Matsuoka, T. Michikami, Y. Mimasu, A. Miura, T. Morota, S. Nakazawa, N. Namiki, H. Noda, R. Noguchi, N. Ogawa, K. Ogawa, T. Okada, C. Okamoto, G. Ono, M. Ozaki, T. Saiki, N. Sakatani, H. Sawada, H. Senshu, Y. Shimaki, K. Shirai, S. Sugita, Y. Takei, H. Takeuchi, S. Tanaka, E. Tatsumi, F. Terui, Y. Tsuda, R. Tsukizaki, K. Wada, S. I. Watanabe, M. Yamada, T. Yamada, Y. Yamamoto, H. Yano, Y. Yokota, K. Yoshihara, M. Yoshikawa, K. Yoshikawa, S. Furuya, K. Hatakeda, T. Hayashi, Y. Hitomi, K. Kumagai, A. Miyazaki, A. Nakato, M. Nishimura, H. Soejima, A. Suzuki, T. Yada, D. Yamamoto, K. Yogata, M. Yoshitake, S. Tachibana, H. Yurimoto, Samples returned from the asteroid Ryugu are similar to Ivuna-type carbonaceous meteorites. *Science* **379**, eabn7850 (2022).
4. G. J. Taylor, The bulk composition of Mars. *Geochemistry* **73**, 401–420 (2013).
5. R. C. Paniello, F. Moynier, P. Beck, J.-A. Barrat, F. A. Podosek, S. Pichat, Zinc isotopes in HEDs: Clues to the formation of 4-Vesta, and the unique composition of Pecora Escarpment 82502. *Geochim. Cosmochim. Acta* **86**, 76–87 (2012).
6. R. C. Paniello, J. M. D. Day, F. Moynier, Zinc isotopic evidence for the origin of the Moon. *Nature* **490**, 376–379 (2012).
7. P. A. Sossi, O. Nebel, H. S. C. O'Neill, F. Moynier, Zinc isotope composition of the Earth and its behaviour during planetary accretion. *Chem. Geol.* **477**, 73–84 (2018).
8. J. M. D. Day, F. Moynier, C. K. Shearer, Late-stage magmatic outgassing from a volatile-depleted Moon. *Proc. Natl. Acad. Sci. U.S.A.* **114**, 9547–9551 (2017).
9. M. Miyamoto, H. Takeda, Evaluation of a crust model of eucrites from the width of exsolved pyroxene. *Geochem. J.* **11**, 161–169 (1977).
10. H. Mori, H. Takeda, Thermal and deformational histories of diogenites as inferred from their microtextures of orthopyroxene. *Earth Planet. Sci. Lett.* **53**, 266–274 (1981).
11. J. J. Papike, C. K. Shearer, M. N. Spilde, J. M. Karner, Metamorphic diogenite Grosvenor Mountains 95555: Mineral chemistry of orthopyroxene and spinel and comparisons to the diogenite suite. *Meteorit. Planet. Sci.* **35**, 875–879 (2000).
12. A. Ruzicka, G. A. Snyder, L. A. Taylor, Vesta as the howardite, eucrite and diogenite parent body: Implications for the size of a core and for large-scale differentiation. *Meteorit. Planet. Sci.* **32**, 825–840 (1997).
13. C. Kato, F. Moynier, M. C. Valdes, J. K. Dhaliwal, J. M. D. Day, Extensive volatile loss during formation and differentiation of the Moon. *Nat. Commun.* **6**, 7617 (2015).
14. E. H. Hauri, A. E. Saal, M. J. Rutherford, J. A. Van Orman, Water in the Moon's interior: Truth and consequences. *Earth Planet. Sci. Lett.* **409**, 252–264 (2015).
15. J.-A. Barrat, A. Yamaguchi, R. C. Greenwood, M. Bohn, J. Cotten, M. Benoit, I. A. Franchi, The Stannern trend eucrites: Contamination of main group eucritic magmas by crustal partial melts. *Geochim. Cosmochim. Acta* **71**, 4108–4124 (2007).
16. P. S. Savage, F. Moynier, M. Boyet, Zinc isotope anomalies in primitive meteorites identify the outer solar system as an important source of Earth's volatile inventory. *Icarus* **386**, 115172 (2022).
17. T. Steller, C. Burkhardt, C. Yang, T. Kleine, Nucleosynthetic zinc isotope anomalies reveal a dual origin of terrestrial volatiles. *Icarus* **386**, 115171 (2022).
18. R. Martins, S. Kuthning, B. J. Coles, K. Kreissig, M. Rehkämper, Nucleosynthetic isotope anomalies of zinc in meteorites constrain the origin of Earth's volatiles. *Science* **379**, 369–372 (2023).
19. M. Paquet, F. Moynier, T. Yokoyama, W. Dai, Y. Hu, Y. Abe, J. Aléon, C. M. Alexander, S. Amari, Y. Amelin, Contribution of Ryugu-like material to Earth's volatile inventory by Cu and Zn isotopic analysis. *Nat. Astron.* **7**, 182–189 (2022).
20. T. Kleine, T. Steller, C. Burkhardt, F. Nimmo, An inner solar system origin of volatile elements in Mars. *Icarus* **397**, 115519 (2023).
21. M. Paquet, P. A. Sossi, F. Moynier, Origin and abundances of volatiles on Mars from the zinc isotopic composition of Martian meteorites. *Earth Planet. Sci. Lett.* **611**, 118126 (2023).
22. A. Trinquier, T. Elliott, D. Ulfbeck, C. Coath, A. N. Krot, M. Bizzarro, Origin of nucleosynthetic isotope heterogeneity in the solar protoplanetary disk. *Science* **324**, 374–376 (2009).
23. J. Render, G. A. Brennecka, C. Burkhardt, T. Kleine, Solar System evolution and terrestrial planet accretion determined by Zr isotopic signatures of meteorites. *Earth Planet. Sci. Lett.* **595**, 117748 (2022).
24. J.-A. Barrat, A. Yamaguchi, R. C. Greenwood, M. Benoit, J. Cotten, M. Bohn, I. A. Franchi, Geochemistry of diogenites: Still more diversity in their parental melts. *Meteorit. Planet. Sci.* **43**, 1759–1775 (2008).
25. F. Moynier, D. Vance, T. Fujii, P. Savage, The isotope geochemistry of zinc and copper. *Rev. Mineral. Geochem.* **82**, 543–600 (2017).
26. H. Chen, P. S. Savage, F.-Z. Teng, R. T. Helz, F. Moynier, Zinc isotope fractionation during magmatic differentiation and the isotopic composition of the bulk Earth. *Earth Planet. Sci. Lett.* **369–370**, 34–42 (2013).
27. G. Budde, F. L. H. Tissot, T. Kleine, R. T. Marquez, Spurious molybdenum isotope anomalies resulting from non-exponential mass fractionation. *Geochemistry* **83**, 126007 (2023).
28. A. Al-Kathiri, B. A. Hofmann, A. J. T. Jull, E. Gnos, Weathering of meteorites from Oman: Correlation of chemical and mineralogical weathering proxies with 14C terrestrial ages and the influence of soil chemistry. *Meteorit. Planet. Sci.* **40**, 1215–1239 (2005).
29. G. Crozaz, C. Floss, M. Wadhwa, Chemical alteration and REE mobilization in meteorites from hot and cold deserts. *Geochim. Cosmochim. Acta* **67**, 4727–4741 (2003).
30. K. Benzerara, F. Guyot, J. A. Barrat, P. Gillet, M. Lesourd, Cristobalite inclusions in the Tatahouine achondrite: Implications for shock conditions. *Am. Mineral.* **87**, 1250–1256 (2002).
31. A. Yamaguchi, J.-A. Barrat, N. Shirai, M. Ebihara, Petrology and geochemistry of Northwest Africa 5480 diogenite and evidence for a basin-forming event on Vesta. *Meteorit. Planet. Sci.* **50**, 1260–1270 (2015).
32. J. M. D. Day, R. J. Walker, L. Qin, D. Rumble Iii, Late accretion as a natural consequence of planetary growth. *Nat. Geosci.* **5**, 614–617 (2012).
33. M. E. Zolensky, M. K. Weisberg, P. C. Buchanan, D. W. Mittlefehldt, Mineralogy of carbonaceous chondrite clasts in HED achondrites and the Moon. *Meteorit. Planet. Sci.* **31**, 518–537 (1996).
34. M. E. Zolensky, R. H. Hewins, D. W. Mittlefehldt, M. M. Lindstrom, X. Xiao, M. E. Lipschutz, Mineralogy, petrology and geochemistry of carbonaceous chondritic clasts in the LEW 85300 polymict eucrite. *Meteoritics* **27**, 596–604 (1992).
35. M. E. Zolensky, D. W. Mittlefehldt, M. E. Lipschutz, M.-S. Wang, R. N. Clayton, T. K. Mayeda, M. M. Grady, C. Pillinger, D. B, CM chondrites exhibit the complete petrologic range from type 2 to 1. *Geochim. Cosmochim. Acta* **61**, 5099–5115 (1997).

36. J.-M. Luck, D. B. Othman, F. Albarède, Zn and Cu isotopic variations in chondrites and iron meteorites: Early solar nebula reservoirs and parent-body processes. *Geochim. Cosmochim. Acta* **69**, 5351–5363 (2005).
37. B. Mahan, F. Moynier, P. Beck, E. A. Pringle, J. Siebert, A history of violence: Insights into post-accretionary heating in carbonaceous chondrites from volatile element abundances, Zn isotopes and water contents. *Geochim. Cosmochim. Acta* **220**, 19–35 (2018).
38. D. Wolf, H. Palme, The solar system abundances of phosphorus and titanium and the nebular volatility of phosphorus. *Meteorit. Planet. Sci.* **36**, 559–571 (2001).
39. R. H. Hewins, M. Bourot-Denise, B. Zanda, H. Leroux, J.-A. Barrat, M. Humayun, C. Göpel, R. C. Greenwood, I. A. Franchi, S. Pont, J.-P. Lorand, C. Cournède, J. Gattacceca, P. Rochette, M. Kuga, Y. Marrocchi, B. Marty, The Paris meteorite, the least altered CM chondrite so far. *Geochim. Cosmochim. Acta* **124**, 190–222 (2014).
40. B. Mahan, J. Siebert, E. A. Pringle, F. Moynier, Elemental partitioning and isotopic fractionation of Zn between metal and silicate and geochemical estimation of the S content of the Earth's core. *Geochim. Cosmochim. Acta* **196**, 252–270 (2017).
41. C. Yang, S.-A. Liu, L. Zhang, Z.-Z. Wang, P.-P. Liu, S.-G. Li, Zinc isotope fractionation between Cr-spinel and olivine and its implications for chromite crystallization during magma differentiation. *Geochim. Cosmochim. Acta* **313**, 277–294 (2021).
42. J. Chikami, M. Miyamoto, H. Takeda, The variation of Zn content in spinel group minerals and daubreelites of primitive achondrites. *Antarct. Meteorite Res.* **12**, 139–150 (1999).
43. F. Moynier, R. C. Paniello, M. Gounelle, F. Albarède, P. Beck, F. Podosek, B. Zanda, Nature of volatile depletion and genetic relationships in enstatite chondrites and aubrites inferred from Zn isotopes. *Geochim. Cosmochim. Acta* **75**, 297–307 (2011).
44. L. J. Bridgestock, H. Williams, M. Rehkämper, F. Larner, M. D. Giscard, S. Hammond, B. Coles, R. Andreasen, B. J. Wood, K. J. Theis, Unlocking the zinc isotope systematics of iron meteorites. *Earth Planet. Sci. Lett.* **400**, 153–164 (2014).
45. J. Chikami, H. Takeda, K. Yugami, T. Mikouchi, M. Miyamoto, Zn abundance in coexisting troilite and spinel in achondrites: Remnant indicative of the primitive source material, in Lunar and Planetary Science Conference, **28**, 225 (1997).
46. E. A. Pringle, F. Moynier, P. Beck, R. Paniello, D. C. Hezel, The origin of volatile element depletion in early solar system material: Clues from Zn isotopes in chondrules. *Earth Planet. Sci. Lett.* **468**, 62–71 (2017).
47. E. van Kooten, F. Moynier, Zinc isotope analyses of singularly small samples (< 5 ng Zn): Investigating chondrule-matrix complementarity in Leoville. *Geochim. Cosmochim. Acta* **261**, 248–268 (2019).
48. K. Righter, M. J. Drake, A magma ocean on Vesta: Core formation and petrogenesis of eucrites and diogenites. *Meteorit. Planet. Sci.* **32**, 929–944 (1997).
49. J.-A. Barrat, A. Yamaguchi, B. Zanda, C. Bollinger, M. Bohn, Relative chronology of crust formation on asteroid Vesta: Insights from the geochemistry of diogenites. *Geochim. Cosmochim. Acta* **74**, 6218–6231 (2010).
50. A. Yamaguchi, J. A. Barrat, M. Ito, M. Bohn, Posteucritic magmatism on Vesta: Evidence from the petrology and thermal history of diogenites. *J. Geophys. Res.* **116**, E08009 (2011).
51. Y. Xue, J. Kang, S. Liao, R. Pang, H. Yu, Z. Zhao, Z. Zhang, B. Miao, W. Hsu, F. Huang, Calcium isotope constraints on the origin of eucrites and diogenites: The role of magma ocean and magmatism. *Earth Planet. Sci. Lett.* **613**, 118171 (2023).
52. K. Zhu, P. A. Sossi, J. Siebert, F. Moynier, Tracking the volatile and magmatic history of Vesta from chromium stable isotope variations in eucrite and diogenite meteorites. *Geochim. Cosmochim. Acta* **266**, 598–610 (2019).
53. K. Zhu, H. Hui, M. Klaver, S. J. Li, L. Chen, W. Hsu, Calcium isotope evolution during differentiation of Vesta and calcium isotopic heterogeneities in the inner solar system. *Geophys. Res. Lett.* **50**, e2022GL102179 (2023).
54. M. Ikramuddin, C. M. Binz, M. E. Lipschutz, Thermal metamorphism of primitive meteorites—II. Ten trace elements in Abee enstatite chondrite heated at 400–1000° C. *Geochim. Cosmochim. Acta* **40**, 133–142 (1976).
55. M. Ikramuddin, S. Matza, M. E. Lipschutz, Thermal metamorphism of primitive meteorites—V. Ten trace elements in Tieschitz H3 chondrite heated at 400–1000° C. *Geochim. Cosmochim. Acta* **41**, 1247–1256 (1977).
56. M. S. Wang, M. E. Lipschutz, Thermally metamorphosed carbonaceous chondrites from data for thermally mobile trace elements. *Meteorit. Planet. Sci.* **33**, 1297–1302 (1998).
57. E. Amsellem, F. Moynier, B. Mahan, P. Beck, Timing of thermal metamorphism in CM chondrites: Implications for Ryugu and Bennu future sample return. *Icarus* **339**, 113593 (2020).
58. F. Moynier, P. Beck, F. Jourdan, Q.-Z. Yin, U. Reimold, C. Koeberl, Isotopic fractionation of zinc in tektites. *Earth Planet. Sci. Lett.* **277**, 482–489 (2009).
59. B. S. Kamber, R. Schoenberg, Evaporative loss of moderately volatile metals from the superheated 1849 Ma Sudbury impact melt sheet inferred from stable Zn isotopes. *Earth Planet. Sci. Lett.* **544**, 116356 (2020).
60. R. Mathur, B. Mahan, M. Spencer, L. Godfrey, N. Landman, M. Garb, D. Graham Pearson, S.-A. Liu, F. E. Oboh-Ikuenobe, Fingerprinting the Cretaceous-Paleogene boundary impact with Zn isotopes. *Nat. Commun.* **12**, 4128 (2021).
61. Y.-A. Brugier, J.-A. Barrat, B. Gueguen, A. Agranier, A. Yamaguchi, A. Bischoff, Zinc isotopic variations in ureilites. *Geochim. Cosmochim. Acta* **246**, 450–460 (2019).
62. J.-P. Toutain, J. Sonke, M. Munoz, A. Nonell, M. Polvé, J. Viers, R. Freydier, F. Sortino, J.-L. Joron, S. Sumarti, Evidence for Zn isotopic fractionation at Merapi volcano. *Chem. Geol.* **253**, 74–82 (2008).
63. J. M. D. Day, F. Moynier, A. P. Meshik, O. V. Pradivtseva, D. R. Petit, Evaporative fractionation of zinc during the first nuclear detonation. *Sci. Adv.* **3**, e1602668 (2017).
64. J. Wimpenny, N. Marks, K. Knight, J. M. Rolison, L. Borg, G. Eppich, J. Badro, F. J. Ryerson, M. Sanborn, M. H. Huyskens, Experimental determination of Zn isotope fractionation during evaporative loss at extreme temperatures. *Geochim. Cosmochim. Acta* **259**, 391–411 (2019).
65. P. A. Sossi, F. Moynier, R. Treilles, M. Mokhtari, X. Wang, J. Siebert, An experimentally-determined general formalism for evaporation and isotope fractionation of Cu and Zn from silicate melts between 1300 and 1500 C and 1 bar. *Geochim. Cosmochim. Acta* **288**, 316–340 (2020).
66. D. D. Bogard, D. H. Garrison, 39Ar-40Ar ages of eucrites and thermal history of asteroid 4 Vesta. *Meteorit. Planet. Sci.* **38**, 669–710 (2003).
67. D. Bogard, D. Garrison, Ar-Ar impact heating ages of eucrites and timing of the LHB, in Lunar and Planetary Science Conference (No. JSC-17610. 2009).
68. J. A. Barrat, B. Zanda, F. Moynier, C. Bollinger, C. Liorzou, G. Bayon, Geochemistry of CI chondrites: Major and trace elements, and Cu and Zn Isotopes. *Geochim. Cosmochim. Acta* **83**, 79–92 (2012).
69. H. S. C. O'Neill, H. Palme, Collisional erosion and the non-chondritic composition of the terrestrial planets. *Philos. Trans. A Math. Phys. Eng. Sci.* **366**, 4205–4238 (2008).
70. J. Siebert, P. A. Sossi, I. Blanchard, B. Mahan, J. Badro, F. Moynier, Chondritic Mn/Na ratio and limited post-nebular volatile loss of the Earth. *Earth Planet. Sci. Lett.* **485**, 130–139 (2018).
71. Y. Hu, F. Moynier, M. Bizzarro, Potassium isotope heterogeneity in the early Solar System controlled by extensive evaporation and partial recondensation. *Nat. Commun.* **13**, 1–10 (2022).
72. B. Wang, F. Moynier, Y. Hu, Rubidium isotopic compositions of angrites controlled by extensive evaporation and partial recondensation. *Proc. Natl. Acad. Sci. U.S.A.* **121**, e2311402121 (2024).
73. N. Dauphas, N. X. Nie, M. Blanchard, Z. J. Zhang, H. Zeng, J. Y. Hu, M. Meheut, C. Visscher, R. Canup, T. Hopp, The extent, nature, and origin of K and Rb depletions and isotopic fractionations in Earth, the Moon, and other planetary bodies. *Planet. Sci. J.* **3**, 29 (2022).
74. A. M. Davis, F. M. Richter, Condensation and Evaporation of Solar System Materials. In *Treatise on geochemistry* (Second Edition) H. D. Holland and K. K. Turekian (eds.) (Elsevier, Oxford, 2014).
75. E. D. Young, A. Shahar, F. Nimmo, H. E. Schlichting, E. A. Schauble, H. Tang, J. Labidi, Near-equilibrium isotope fractionation during planetesimal evaporation. *Icarus* **323**, 1–15 (2019).
76. Z. Tian, H. Chen, B. Fegley, K. Lodders, J.-A. Barrat, J. M. D. Day, K. Wang, Potassium isotopic compositions of howardite-eucrite-diogenite meteorites. *Geochim. Cosmochim. Acta* **266**, 611–632 (2019).
77. E. A. Pringle, F. Moynier, Rubidium isotopic composition of the Earth, meteorites, and the Moon: Evidence for the origin of volatile loss during planetary accretion. *Earth Planet. Sci. Lett.* **473**, 62–70 (2017).
78. Z. Tian, T. Magna, J. M. D. Day, K. Mezger, E. E. Scherer, K. Lodders, R. C. Hin, P. Koefoed, H. Bloom, K. Wang, Potassium isotope composition of Mars reveals a mechanism of planetary volatile retention. *Proc. Natl. Acad. Sci. U.S.A.* **118**, e2101155118 (2021).
79. M. Schiller, M. Bizzarro, V. A. Fernandes, Isotopic evolution of the protoplanetary disk and the building blocks of Earth and the Moon. *Nature* **555**, 507–510 (2018).
80. J. A. Barrat, N. Dauphas, P. Gillet, C. Bollinger, J. Etoubleau, A. Bischoff, A. Yamaguchi, Evidence from Tm anomalies for non-CI refractory lithophile element proportions in terrestrial planets and achondrites. *Geochim. Cosmochim. Acta* **176**, 1–17 (2016).
81. A. Johansen, T. Ronnet, M. Bizzarro, M. Schiller, M. Lambrechts, Å. Nordlund, H. Lammer, A pebble accretion model for the formation of the terrestrial planets in the Solar System. *Sci. Adv.* **7**, eabc0444 (2021).
82. C. Burkhardt, F. Spitzer, A. Morbidelli, G. Budde, J. H. Render, T. S. Kruijer, T. Kleine, Terrestrial planet formation from lost inner solar system material. *Sci. Adv.* **7**, eabj7601 (2021).
83. M.-L. Steinmeyer, P. Woitke, A. Johansen, Sublimation of refractory minerals in the gas envelopes of accreting rocky planets. *Astron. Astrophys.* **677**, A181 (2023).
84. F. Moynier, M. Le Borgne, High precision zinc isotopic measurements applied to mouse organs. *J. Vis. Exp.* , e52479 (2015).
85. K. J. R. Rosman, A survey of the isotopic and elemental abundance of zinc. *Geochim. Cosmochim. Acta* **36**, 801–819 (1972).

Acknowledgments: We thank P. Burckel, D. Rigoussen, and T.-H. Luu for the help on chemistry work and J. Siebert and R. Tartèse for discussions. **Funding:** F.M. acknowledges the ERC grant

101001282 (METAL). Parts of this work were supported by IPGP multidisciplinary program PARI, by Region Île-de-France SESAME grant nos. 12015908 and EX047016, and the IdEx Université de Paris grant ANR-18-IDEX-0001 and the DIM ACAV+. L.F. thanks the China Scholarship Council for a Ph.D. fellowship (#202004910297). **Author contributions:** Conceptualization: F.M. and L.F. Methodology: L.F., F.M., J.-A.B., A.Y., and M.P. Investigation: L.F., F.M., J.-A.B., and M.C. Visualization: L.F. Supervision: F.M., M.C., and J.-A.B. Writing–original draft: L.F. Writing–review and editing: All authors. **Competing interests:** The authors declare that they have no competing interests. **Data and materials availability:** All data needed to evaluate the conclusions in the paper are present in the paper and/or the Supplementary Materials.

Submitted 29 September 2023
Accepted 10 July 2024
Published 14 August 2024
10.1126/sciadv.adl1007